Compact optical 90° hybrid employing a tapered 2×4 MMI coupler serially connected by a 2×2 MMI coupler

Seok-Hwan Jeong* and Ken Morito

Fujitsu Laboratories Ltd., 10-1 Morinosato-Wakamiya, 243-0122, Japan
**jeong.sh@jp.fujitsu.com*

Abstract: We propose a novel optical 90° hybrid employing a paired-interference-based tapered 2×4 multimode interference coupler and a 2×2 multimode interference coupler. It was experimentally shown that the proposed 90° hybrid has very short device length of less than 227 μm and is never accompanied by any waveguide intersections for coupling to balanced photodiodes. The proposed device exhibited quadrature phase response with a common-mode rejection ratio of more than 20dB and a phase deviation of less than 5° over C-band spectral range.

OCIS codes: (130.3120) Integrated optics devices; (230.7370) Waveguides.

References and links

1. K. Kikuchi, "Phase-diversity homodyne detection of multilevel optical modulation with digital carrier phase estimation," IEEE J. Sel. Top. Quantum Electron. **12**(4), 563–570 (2006).
2. M. Seimetz, and C. M. Weinert, "Options, feasibility and availability of 2×4 90° hybrids for coherent optical systems," J. Lightwave Technol. **24**(3), 1317–1322 (2006).
3. D. Hoffmann, H. Heidrich, G. Wenke, R. Langenhorst, and E. Dietrich, "Integrated optics eight-port 90° hybrid on $LiNbO_3$," J. Lightwave Technol. **7**(5), 794–798 (1989).
4. R. Kunkel, H. G. Bach, D. Hoffmann, C. M. Weinert, I. Molina-Fernandez, and R. Halir, "First monolithic InP-based 90° hybrid OEIC comprising balanced detectors for 100GE coherent frontends," Proc. IPRM 2009, paper TuB2.2 (2009).
5. C. R. Doerr, D. M. Gill, A. H. Gnauck, L. L. Buhl, P. J. Winzer, M. A. Cappuzzo, A. Wong-Foy, E. Y. Chen, and L. T. Gomez, "Monolithic demodulator for 40-Gb/s DQPSK using a star coupler," J. Lightwave Technol. **24**(1), 171–174 (2006).
6. C. R. Doerr, L. Zhangl, S. Chandrasekhar, and L. L. Buhl, "Monolithic DQPSK receiver in InP with low polarization sensitivity," IEEE Photon. Technol. Lett. **19**(21), 1765–1767 (2007).
7. L. Zimmermann, K. Voigt, G. Winzer, K. Petermann, and C. M. Weinert, "C-band optical 90°-hybrids based on Silicon-on-insulator 4×4 waveguide coupler," IEEE Photon. Technol. Lett. **21**(3), 143–145 (2009).
8. H. G. Bach, A. Matiss, C. C. Leonhardt, R. Kunkel, D. Schmidt, M. Schell, and A. Umbach, "Monolithic 90° hybrid with balanced pin photodiodes for 100 Gbit/s PM-QPSK receiver applications," Proc. OFC 2009, paper OMK5 (2009).
9. M. Baudreau, M. Poirier, G. Yoffe, and B. Pezeshki, "An integrated InP coherent receiver for 40 and 100 Gb/sec telecommunications systems," Proc. OFC 2009, paper OMK6 (2009).
10. S.-H. Jeong, and K. Morito, "Optical 90° hybrid with broad operating bandwidth of 94 nm," Opt. Lett. **34**(22), 3505–3507 (2009).
11. L. B. Soldano, and C. M. Pennings, "Optical multi-mode interference devices based on self-imaging: Principles and Applications," J. Lightwave Technol. **13**(4), 615–627 (1995).
12. D. S. Levy, R. Scarmozzino, and R. M. Osgood, "Length reduction of tapered N×N MMI devices," IEEE Photon. Technol. Lett. **10**(6), 830–832 (1998).

1. Introduction

As one of efficient methods to be able to maximize spectral efficiencies and receiver sensitivities, multilevel transmission systems employing quadrature phase shift keyed (QPSK) modulation formats have been actively investigated [1]. An optical 90° hybrid works as a demodulator of the QPSK modulated signals [2], thus enabling to detect phase-coded information through optoelectronic conversion by two pairs of balanced photodiodes (PDs).

#121211 - $15.00 USD Received 9 Dec 2009; revised 24 Dec 2009; accepted 30 Dec 2009; published 17 Feb 2010

Compared with bulk-optics-based 90° hybrids, optical waveguide-based 90° hybrids are more attractive for compactness of the device and monolithic integration with balanced PDs in coherent receivers. To date, there have been many reports on the waveguide-based 90° hybrids using 2×2 optical couplers and phase delays [3,4], a star coupler [5,6], a 4×4 multimode interference (MMI) coupler [7–9]. Recently, successful optical quadrature behaviors were experimentally demonstrated in coherent detection schemes monolithically integrated with balanced PDs [4,6,8,9].

However, such coherent detection schemes using conventional waveguide-based 90° hybrids inevitably required waveguide intersections [4,8], which might cause excess losses and crosstalk at the cross junction area. In an effort to overcome a drawback related to the waveguide intersection, we proposed a novel optical 90° hybrid consisting of a paired interference (PI) based 2×4 MMI coupler, a phase shifter and a 2×2 MMI coupler [10]. Hereafter, we call the optical 90° hybrid Type-I scheme. In Ref. 10, we experimentally verified that the Type-I scheme exhibits quadrature phase response without employing any waveguide intersection areas. However, the size of the Type-I scheme was inherently larger than the 4×4 MMI coupler-based devices by a factor of ~1.3. Furthermore, in order to achieve quadrature phase response with low crosstalk, an additional phase shifter should be located between the PI-based 2×4 MMI coupler and the 2×2 MMI coupler in the Type-I scheme.

Here, we propose a novel optical 90° hybrid that does not need any waveguide intersections and the additional phase shifter for implementing coherent detection. The proposed optical 90° hybrid is composed of a PI-based tapered 2×4 MMI coupler serially connected by a 2×2 MMI coupler. Since the proposed device never requires any additional phase shifters to suppress crosstalk for the demodulated signal with a quadrature phase, the device becomes much simpler in design and more compact in size. We numerically analyze and experimentally demonstrate quadrature phase operation with a low wavelength sensitive loss (<1dB), a high common-mode rejection ratio (>20dB) and a low phase deviation ($|\Delta\phi|<5°$) over full C-band spectral range.

2. Basic MMI theory

Here, we briefly explain basic theory related to self imaging in the MMI region [11]. Usually, a beat length (L_π) in the MMI region is given by

$$L_\pi = \frac{\pi}{\beta_0 - \beta_1} \tag{1}$$

where β_0 and β_1 indicate the propagation constant of a fundamental mode and a first-order mode, respectively. Considering a strongly lateral guiding structure such as a deep-ridge waveguide, L_π can be approximated as

$$L_\pi \cong \frac{4 \cdot N_{eq} \cdot W_{eff}^2}{3 \cdot \lambda} \tag{2}$$

where N_{eq} and λ indicate a refractive index and a wavelength, respectively. W_{eff} stands for an effective MMI width that takes into account mode penetration depth of each mode field. In the case of the aforementioned strongly lateral guiding structure, we can regard W_{eff} as a physical MMI width itself due to its strong lateral mode confinement. Consequently, the propagation constant difference between a fundamental mode and an arbitrary higher-order mode can be represented as

$$\beta_0 - \beta_\nu \cong \frac{\nu(\nu+2)\pi\lambda}{4 \cdot N_{eq} \cdot W_{eff}^2} = \frac{\nu(\nu+2)\pi}{3L_\pi} \tag{3}$$

#121211 - $15.00 USD Received 9 Dec 2009; revised 24 Dec 2009; accepted 30 Dec 2009; published 17 Feb 2010

where ν indicates a mode number. In this case, the value of $(\beta_0-\beta_\nu)$ shown in Eq. (3) governs a self imaging property in the MMI region. When the MMI width is constant, a net relative phase change along the MMI length ($\Delta\rho$) can be simply expressed as

$$\Delta\rho = \left(\beta_0 - \beta_\nu\right)\cdot L_{MMI} \tag{4}$$

where L_{MMI} is the MMI length. On the other hand, if the MMI width is modulated along the propagation direction, the value of $(\beta_0-\beta_\nu)$ varies locally. Thus, $\Delta\rho$ should be represented by taking into account the local variation of $(\beta_0-\beta_\nu)$ along the propagation direction [12],

$$\Delta\rho = \int_0^{L_{MMI}} \left(\beta_0 - \beta_\nu\right) dz = \frac{\nu\left(\nu+2\right)\pi\lambda}{4\cdot N_{eq}} \int_0^{L_{MMI}} \frac{dz}{W_M^2(z)} \tag{5}$$

where $W_M(z)$ indicates a modulation function of the MMI width. Consequently, depending on $W_M(z)$, the optimized imaging length and the phase relation of the MMI coupler will be different.

3. Theoretical Consideration

3.1. Optical 90° hybrid based on the Type-I scheme [Ref 10.]

Here, we briefly mention the optical 90° hybrid based on the Type-I scheme. In Ref. 10, we theoretically and experimentally verified that the optical demodulation can be implemented without any waveguide intersections in the coherent detection scheme including balanced PDs. We briefly explain the structure of the Type-I scheme, comparing with the conventional 4×4 MMI coupler.

Figure 1 shows schematic diagrams of optical 90° hybrids based on the Type-I scheme (a) and the conventional 4×4 MMI coupler (b). As shown in Fig. 1(a), the Type-I scheme consists of a 2×4 MMI coupler, a phase shifter and a 2×2 MMI coupler. It is important to note that the 2×4 MMI coupler shown in Fig. 1(a) is based on the restricted excitation of modes [11], while the 4×4 MMI coupler shown in Fig. 1(b) is based on general excitation of modes [11].

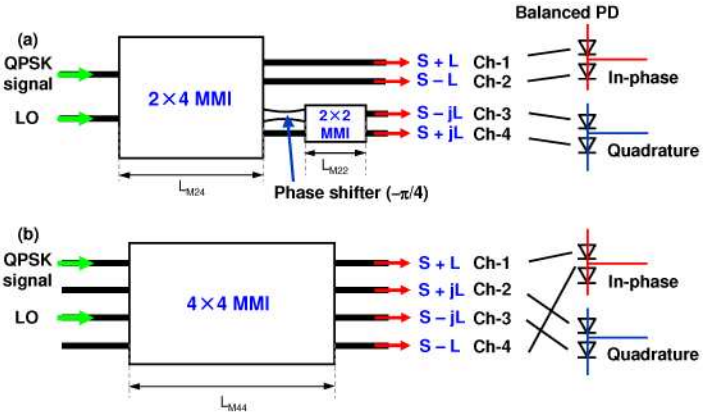

Fig. 1. Schematic diagrams of a coherent detection scheme employing the Type-I scheme (a) and the conventional 4×4 MMI coupler

The operation principle of the Type-I scheme can be explained as follows. When the QPSK signal and the local oscillator (LO) light are incident on the Type-I scheme, each of mutually adjacent two output pairs of the 2×4 MMI coupler show In-phase relation, because the 2×4 MMI coupler works as a 180° hybrid. Then the phase relation at the output components coupled to the 2×2 MMI coupler is rotated by 90° through the modal interference at the 2×2 MMI coupler, which allows us to discriminate the signal with quadrature phase relation. As shown in Fig. 1(a), the output phase relation of the Type-I scheme is given by

#121211 - $15.00 USD Received 9 Dec 2009; revised 24 Dec 2009; accepted 30 Dec 2009; published 17 Feb 2010

S+L for Ch-1, S–L for Ch-2, S–jL for Ch-3 and S+jL for Ch-4, which enables us to directly connect the 90° hybrid output channels to balanced PDs without accompanying any waveguide intersections. The phase shifter shown in Fig. 1(a) plays a major role in adjusting phase matching relation between the 2×4 MMI coupler and the 2×2 MMI coupler. In the Type-I scheme, the phase shifter is absolutely required to minimize the excess losses and the crosstalk for the demodulated signal with a quadrature phase. As a result of analytical calculations, the excess losses and the crosstalk level of the demodulated signal with a quadrature phase tends to be minimized when the following relation is satisfied by the phase shifter,

$$\theta_{Phase} = -\frac{\pi}{4} \tag{6}$$

where θ_{Phase} indicates the amount of phase change at the phase shifter shown in Fig. 1(a). In other words, if the phase shifter satisfies the relation shown in Eq. (6), we can achieve a perfect constructive interference at the output Ch-3 (or Ch-4) and a perfect destructive interference at the output Ch-4 (or Ch-3) in the 2×2 MMI coupler in the Type-I scheme, thus enabling to avoid the degradation of detection efficiencies at the Quadrature channels.

Figure 2 shows the device length (L_{Device}) relation between the Type-I scheme and the 4×4 MMI coupler as a function of the narrowest gap between output waveguide arrays (Gap). Usually, due to different mechanism of mode excitations in the MMI regions, the input and output channel positions of the PI-based MMI coupler are inherently different from those of the general interference (GI) based MMI coupler. In this case, Gap is always smaller in the PI-based MMI coupler than in the GI-based MMI coupler [10]. Since the available Gap is directly influenced by fabrication technologies, the comparison of the device size between the PI-based MMI coupler and the GI-based MMI coupler should be made under the same value of Gap.

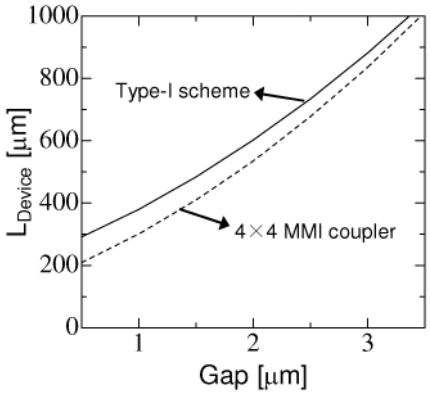

Fig. 2. Device length (L_{Device}) relation between the Type-I scheme and the 4×4 MMI coupler

In this case, L_{Device} of the 4×4 MMI coupler is identical to the 4×4 MMI length (L_{M44}). Meanwhile, L_{Device} of the Type-I scheme corresponds to the sum of the 2×4 MMI length (L_{M24}), the phase shifter length (L_{PS}) and the 2×2 MMI length (L_{M22}) where L_{PS} is assumed to be 50 μm. As clearly seen in Fig. 2, L_{Device} of the Type-I scheme is always larger than that of the 4×4 MMI coupler by a factor of 1.2~1.3. When we set Gap to be 1.1 μm, L_{Device} is determined to be ~399.8 μm for the Type-I scheme and ~321.4 μm for the 4×4 MMI coupler. In addition, the design of the 2×4 MMI coupler and the phase shifter in the Type-I scheme should be independently optimized enough to suppress the crosstalk at the Quadrature channels, which makes the device design somewhat complicated.

#121211 - $15.00 USD Received 9 Dec 2009; revised 24 Dec 2009; accepted 30 Dec 2009; published 17 Feb 2010

3.2. Proposed optical 90° hybrids

Figure 3 shows a schematic drawing of a coherent detection scheme using a proposed optical 90° hybrid. Hereafter, we call the proposed 90° hybrid Type-II scheme. As shown in Fig. 3, the Type-II scheme consists of a linear-tapered 2×4 MMI coupler and a 2×2 MMI coupler. It should be noted that the linear-tapered 2×4 MMI coupler is based on the restricted excitation of modes. Noticeable difference of the Type-II scheme to the Type-I scheme is the shape of the 2×4 MMI coupler and the absence of the phase shifter between the 2×4 MMI coupler and the 2×2 MMI coupler. Since the optical 90° hybrid inherently has the number of input channels less than that of output channels, the input MMI width (W_{MS}) can be narrower than the output MMI width (W_{MF}), thus enabling to form the linear-tapered MMI structure as schematically shown in Fig. 3.

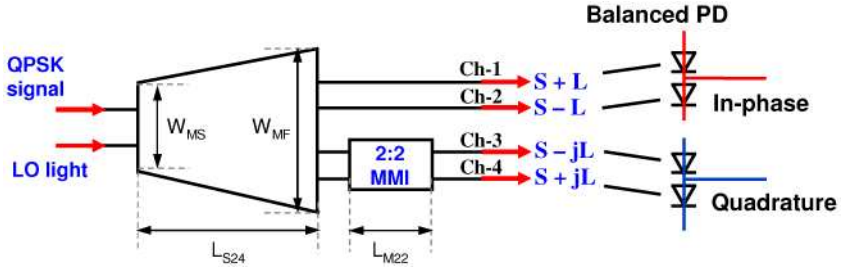

Fig. 3. Schematic diagram of a coherent detection scheme consisting of the proposed 90° hybrid (the Type-II scheme) and balanced PDs

On the other hand, the tapered shape of the 2×4 MMI coupler also contributes to control of relative phase differences between the output channels of the 2×4 MMI coupler. In other words, the four images formed at the output end of the tapered MMI region have different phase tilted angles, which makes it possible to adjust the relative phase differences between four output components. In this case, the required condition shown in Eq. (6) becomes unnecessary, if we add an extra phase change of $-\pi/4$ to the relative phase difference between Ch-3 and Ch-4 at the rectangular shaped 2×4 MMI coupler. This means that no additional phase shifter will be needed to suppress the crosstalk at the Quadrature channel. The advantage of the absence of the phase shifter allows us to directly connect the linear-tapered 2×4 MMI coupler to the 2×2 MMI coupler without using the access waveguide arrays, as schematically shown in Fig. 4.

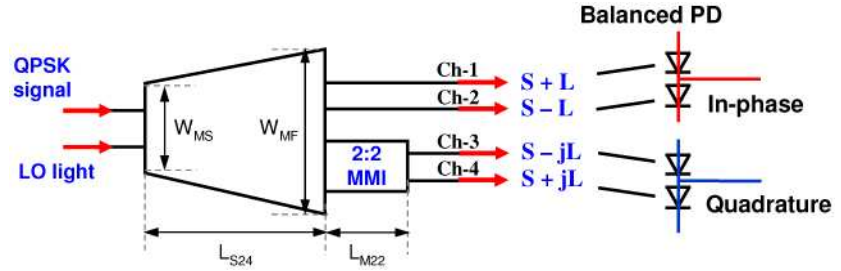

Fig. 4. Schematic diagram of a coherent detection scheme consisting of the proposed 90° hybrid (the Type-II scheme without using access waveguides) and balanced PDs

Consequently, compared with the Type-I scheme, the Type-II scheme shown in Fig. 4 can make the optical 90° hybrid more compact in size and much simpler in design. In case of the Type-II scheme, the modulation function of the linear-tapered MMI coupler is given by

$$W_M(z) = W_{MS} + (W_{MF} - W_{MS})\frac{z}{L_{S24}} \tag{7}$$

#121211 - $15.00 USD Received 9 Dec 2009; revised 24 Dec 2009; accepted 30 Dec 2009; published 17 Feb 2010

where L_{S24} represents the length of the linear-tapered 2×4 MMI coupler. By substituting Eq. (7) in Eq. (5), the net value $<\beta_0-\beta_v>$ can be expressed as,

$$\left\langle \beta_0 - \beta_v \right\rangle = \frac{\nu(\nu+2)\pi\lambda}{4 \cdot N_{eq} \cdot W_{MF}^2} \chi^{ST} \tag{8}$$

$$\chi^{ST} = \frac{W_{MF}}{W_{MS}} \tag{9}$$

where χ^{ST} stands for a proportional constant that is dependent of $W_M(z)$. By using Eqs. (8) and (9), we can define the beat length of the linear-tapered 2×4 MMI coupler (L_π^{ST}) as follows,

$$L_\pi^{ST} = \frac{L_\pi}{\chi^{ST}} \tag{10}$$

Thus, the desired MMI length can be reduced in proportion to χ^{ST}. It should be noted that the above-mentioned analytical formula except Eq. (6) are approximations validated under the condition that all effective MMI widths (W_{eff}) for each excited mode at the MMI region are identical, and each propagation constant for arbitrary modes (β_v) is treated as the Taylor series. Although these analytical approximations normally give insight to determine the required imaging length of the MMI device, we need to utilize a more advanced calculation technique to evaluate amplitude and phase behaviors of the mode interferences in the tapered MMI coupler, because the tapered MMI coupler is normally accompanied by the mode conversion as well as the mode interference along the interaction length, and the validity of the approximated β_v is not assured any longer.

In order to accurately calculate the amplitude and phase characteristics of the linear-tapered MMI coupler, numerical simulation based on a 2-dimensional beam propagation method (2D-BPM) was utilized. In the 2D-BPM simulation, the Pade approximation (4,4) was utilized to minimize phase errors in the tapered region.

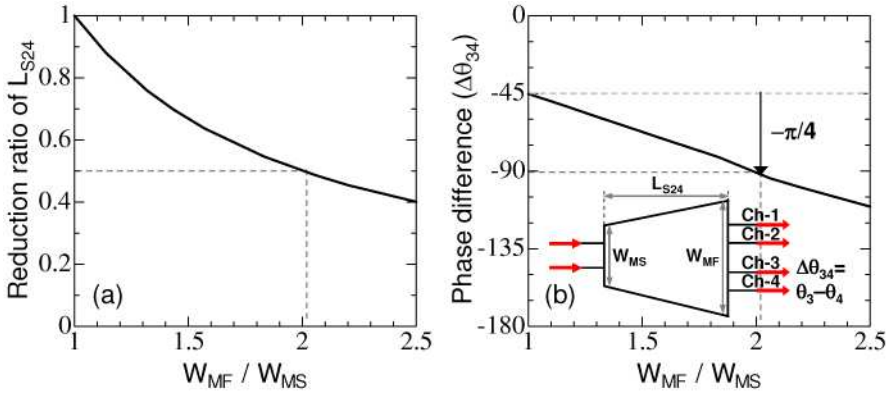

Fig. 5. Calculated reduction ratio of L_{S24} (a) and calculated relative phase difference between Ch-3 and Ch-4 ($\Delta\theta_{34}$) of the linear-tapered 2×4 MMI coupler when the QPSK signal and the LO have the phase difference ($\Delta\Phi$) of $-\pi/2$ (b) as a function of W_{MF}/W_{MS}

Figure 5 shows the calculated reduction ratio of L_{S24} (a) and the calculated relative phase difference between Ch-3 and Ch-4 ($\Delta\theta_{34}$) of the linear-tapered 2×4 MMI coupler when the QPSK signal and the LO have the phase difference ($\Delta\Phi$) of $-\pi/2$ (b) as a function of W_{MF}/W_{MS}. In this case, the rectangular shaped 2×4 MMI coupler whose MMI width keeps constant along the propagation direction corresponds to the case of $W_{MF}/W_{MS}=1$. In Fig. 5(a), the reduction ratio of L_{S24} corresponds to the value of $1/\chi^{ST}$. As W_{MF}/W_{MS} increases (as W_{MS}

#121211 - $15.00 USD Received 9 Dec 2009; revised 24 Dec 2009; accepted 30 Dec 2009; published 17 Feb 2010

decreases) for the fixed value of W_{MF}, the reduction ratio of L_{S24} tends to be decreased, which agreed well with the analytically estimated result based on Eq. (10).

On the other hand, the Type-I scheme shown in Fig. 1(a) required the phase shifter to make the phase matching, which allowed us to minimize the excess losses and the crosstalk at the Quadrature channels. In this case, since the linear-tapered 2×4 MMI coupler can be optimized so that an extra phase change of $-\pi/4$ is provided to the relative phase difference between output Ch-3 and Ch-4 in the rectangular shaped 2×4 MMI coupler ($\Delta\theta_{34}=-\pi/4$), the optical 90° hybrid can be constructed without using the additional phase shifter as schematically shown in Fig. 3 or Fig. 4. As can be seen in Fig. 5(b), in case of the rectangular shaped 2×4 MMI coupler used in Fig. 1, $\Delta\theta_{34}$ is determined to be $-\pi/4$. However, as W_{MF}/W_{MS} increases for a fixed the value of W_{MF}, $\Delta\theta_{34}$ is inclined to be linearly reduced. In this case, when W_{MF}/W_{MS} is set to be 2.06, $\Delta\theta_{34}$ is determined to be $-\pi/2$, together with the length reduction of L_{S24} by 52%. It should be noted that the abilities of omitting the phase shifter and of reducing L_{S24} by the one-half of the comparable taperless device is available for arbitrary W_{MF} or W_{MS} in the linear-tapered 2×4 MMI coupler.

Operation principle of the Type-II scheme is the same as that of the Type-I scheme. Moreover, it should be noted that the relative phase relation at the access waveguides located between the linear-tapered 2×4 MMI coupler and 2×2 MMI coupler keeps constant. Thus, device characteristics of the Type-II scheme won't be directly influenced by the presence of the access waveguides.

Figure 6 shows the simulated light intensity patterns of the Type-II scheme in the absence of the access waveguides. In the simulation, the LO power (P_{LO}) was set to be the same as the signal power (P_S), and the parameters of the linear-tapered 2×4 MMI coupler and the 2×2 MMI couple were optimized for the wavelength of 1.55 μm and a linearly polarized TE-mode. W_{MF} was set to be 18.6 μm. Thus, W_{MS} was optimized to 9.02 μm according to Eq. (9) under the condition of $\chi^{ST}=2.06$.

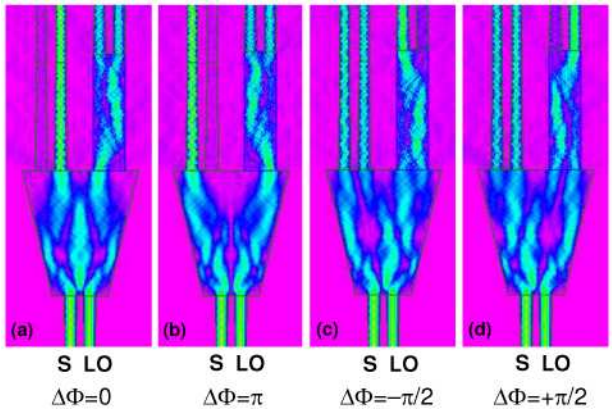

Fig. 6. Simulated transmission characteristics of the Type-II scheme in the absence of the access waveguides for (a) $\Delta\Phi=0$, (b) $\Delta\Phi=\pi$, (c) $\Delta\Phi=-\pi/2$, and (b) $\Delta\Phi=+\pi/2$. The amplitude for the LO was set to be identical to that of the signal.

As seen in Fig. 6, the output field distribution of the Type-II scheme obviously different against $\Delta\Phi$. In Figs. 6(a) and (b), when $\Delta\Phi=0$ (rad.) or π (rad.), the output intensity ratio for each output channel is given by (a) 0:2:1:1 and (b) 2:0:1:1, respectively. Meanwhile, as can be seen in Figs. 6(c) and (d), when $\Delta\Phi=-\pi/2$ (rad.) or $+\pi/2$ (rad.), the output intensity ratio is given by (c) 1:1:2:0 and (d) 1:1:0:2, respectively.

#121211 - $15.00 USD Received 9 Dec 2009; revised 24 Dec 2009; accepted 30 Dec 2009; published 17 Feb 2010

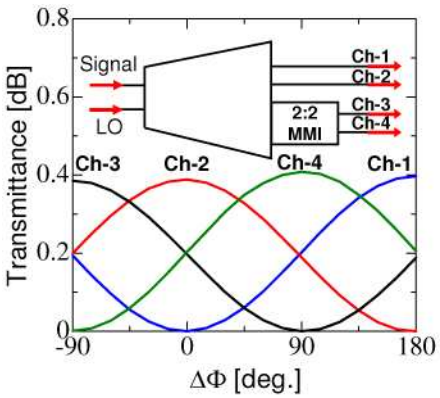

Fig. 7. Calculated transmission spectra of the Type-II scheme shown in Fig. 6 as a function of the phase difference between the signal and the LO (ΔΦ)

Figure 7 shows the calculated transmittances of the Type-II scheme shown in Fig. 6 when the linear-tapered shape (W_{MF}/W_{MS}) was optimized to satisfy the relation of χ^{ST}=2.06. As clearly seen in Fig. 7, there is neither an excess loss nor crosstalk for the signal with a quadrature phase (ΔΦ=–90° and +90°). This is because the phase matching was made by optimizing the linear-tapered shape (W_{MF}/W_{MS}). Unlike the case of the 4×4 MMI coupler, π-phase differences are clearly shown in the output pairs of Ch-1 and 2, and Ch-3 and 4, which enables us to directly connect the output waveguides to the balanced PDs without accompanying any waveguide intersections.

As mentioned before, device characteristics of the Type-II scheme will be little influenced by the presence of the access waveguides if the linear-tapered 2×4 MMI coupler is optimized to satisfy the relation of $\Delta\theta_{34}= -\pi/2$ (rad.). We numerically analyzed wavelength sensitivities on amplitude and phase characteristics of the Type-II schemes. Figure 8 shows the transmission spectra calculated by the 2D-BPM when an optical signal is incident on one input port of the Type-II schemes in the presence of the 50-μm-long access waveguides (a) and the Type-II scheme in the absence of the access waveguides (b). In the simulation, the calculation parameters are the same as those used in Fig. 6. As can be seen in Fig. 8, either proposed scheme operates as a 6 dB power splitter within the C-band spectral range. There is little noticeable difference on spectral characteristics between the Type-II schemes shown in Figs. 8(a) and (b), which verifies the access waveguides have a little effect on the amplitude characteristics of the Type-II scheme. Meanwhile, in either case, a wavelength sensitive loss is less than 1dB for each output channel within the C-band spectral range. It should be noted that either proposed scheme experience not only the splitting loss of 6dB but also the excess loss of ~1.3dB, which originates from the mode conversion in the linear-tapered region and is normally proportional to the reduction ratio of L_{S24}.

Similar to the case of the amplitude characteristics, phase characteristics of the Type-II scheme is little influenced by the access waveguides. Figure 9 shows the calculated relative phase deviation from the quadrature phase relation ($\Delta\phi$) of the Type-II scheme in the presence of the using 50-μm-long access waveguides (a) and the Type-II scheme in the absence of the access waveguides (b). As shown in Fig. 9, either proposed scheme exhibits $|\Delta\phi|$ of <5° within the C-band spectral range, thus enabling to use as a QPSK demodulator over 40-nm-wide wavelength span.

#121211 - $15.00 USD Received 9 Dec 2009; revised 24 Dec 2009; accepted 30 Dec 2009; published 17 Feb 2010

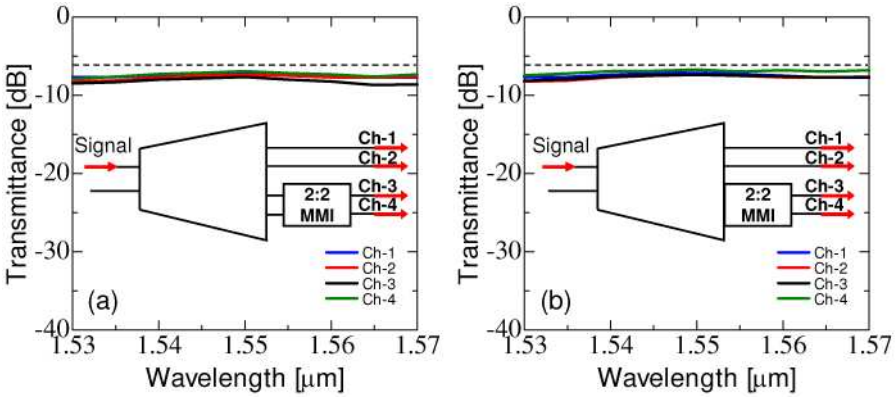

Fig. 8. Calculated transmission spectra of (a) the Type-II scheme in the presence of the 50-μm-long access waveguides and (b) the Type-II scheme in the absence of the access waveguides within the C-band spectral range

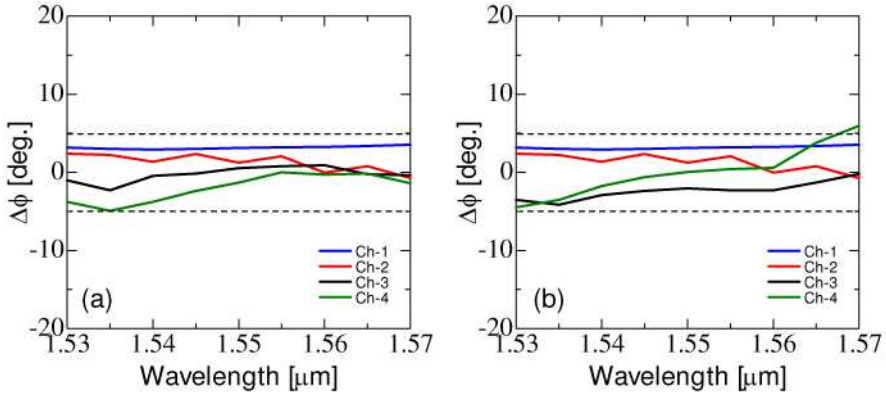

Fig. 9. Calculated relative phase deviation from the quadrature phase relation (Δϕ) of (a) the Type-II scheme in the presence of the 50-μm-long access waveguides and (b) the Type-II scheme in the absence of the access waveguides within the C-band spectral range

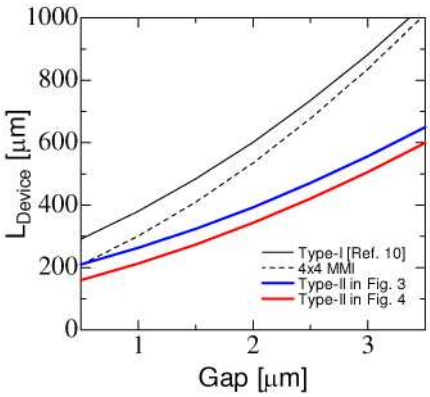

Fig. 10. Device length (L_{Device}) relation between the Type-I scheme, the Type-II schemes and the conventional 4×4 MMI coupler

Figure 10 shows the estimated L_{Device} for several types of optical 90° hybrids as a function of Gap. In the case of the Type-II scheme including the access waveguides, the access waveguide length was supposed to be 50 μm. As can be clearly seen Fig. 10, compared with

#121211 - $15.00 USD Received 9 Dec 2009; revised 24 Dec 2009; accepted 30 Dec 2009; published 17 Feb 2010

the Type-I scheme and the 4×4 MMI coupler, the Type-II schemes exhibit shorter L_{Device} irrespective of Gap. As clearly seen in Figs. 8 and 9, since there is little noticeable dependence of the access waveguides in the Type-II scheme on amplitude and phase characteristics, the Type-II scheme in the absence of the access waveguides is most promising for compactness of the device among four kinds of optical 90° hybrids. When we set Gap to be 1.1 μm, L_{Device} of the Type-II scheme without using the access waveguides is determined to be ~225 μm, which is shorter than the case of the Type-I scheme by a factor of ~1.8.

4. Experimental results

4.1. Fabrication of the device

Based on the theoretical considerations, the Type-II scheme was fabricated on an InP wafer with a 0.3-μm-thick GaInAsP core layer (λ_g=1.3 μm). Waveguide patterns are directly formed by photolithography. Figure 11 shows an SEM picture of the fabricated deep-ridge waveguide with W=2.0 μm. As shown in Fig. 11, using a mask pattern of a predeposited SiO_2 layer, deep-ridge waveguide stripes were formed by using reactive ion etching. Subsequently, the InP substrates for both samples were polished and cleaved.

Figure 12 shows a top-view photograph of the Type-II scheme. The device parameters of the Type-II scheme were set to be the same as those used in the BPM simulations. In the Type-II scheme shown in Fig. 12, we used the GI-based 2×2 MMI coupler for compactness of the device. In this case, L_{Device} was 227 μm in which L_{S24}, L_{M22}, and Gap were set to 116 μm, 111 μm and 1.1 μm, respectively.

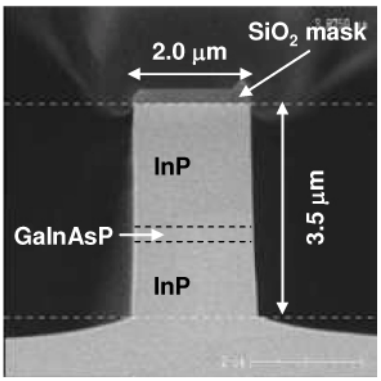

Fig. 11. SEM picture of the fabricated deep etched ridge waveguide with W=2.0 μm.

Fig. 12. Top-view photograph of the proposed 90° hybrid employing the Type-II scheme without using the access waveguides between the linear-tapered 2×4 MMI coupler and the 2×2 MMI coupler

#121211 - $15.00 USD Received 9 Dec 2009; revised 24 Dec 2009; accepted 30 Dec 2009; published 17 Feb 2010

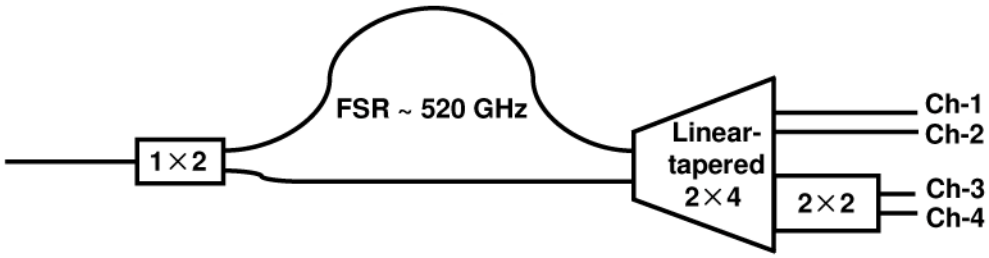

Fig. 13. Schematic drawing of the delayed Mach-Zehnder interferometer integrated Type-II scheme without using the access waveguides

In addition, to experimentally evaluate the phase characteristics of the devices, we also designed and fabricated a test structure in which a delayed Mach-Zehnder interferometer is directly coupled to both devices. Figure 13 shows the schematic drawing of the fabricated test structures for the Type-II scheme. A free-spectral range of the delayed Mach-Zehnder interferometer was designed to be ~520 GHz. In the delayed interferometer, we used the 1×2 MMI coupler based on the symmetric excitation of modes [11]. The total chip size including fan-out regions for a fiber butt-coupling measurement was 1.7×0.25 mm^2.

4.2. Measurement

To measure the transmission spectra of the fabricated devices, we used an amplified spontaneous emission of a semiconductor optical amplifier as a light source. The input polarization state was adjusted to be a linearly polarized TE-mode through a polarization controller. The input light was butt coupled to the input port of the device through a single-mode lensed fiber. The output light was butt-coupled to a single-mode lensed fiber and then measured with a spectrum analyzer.

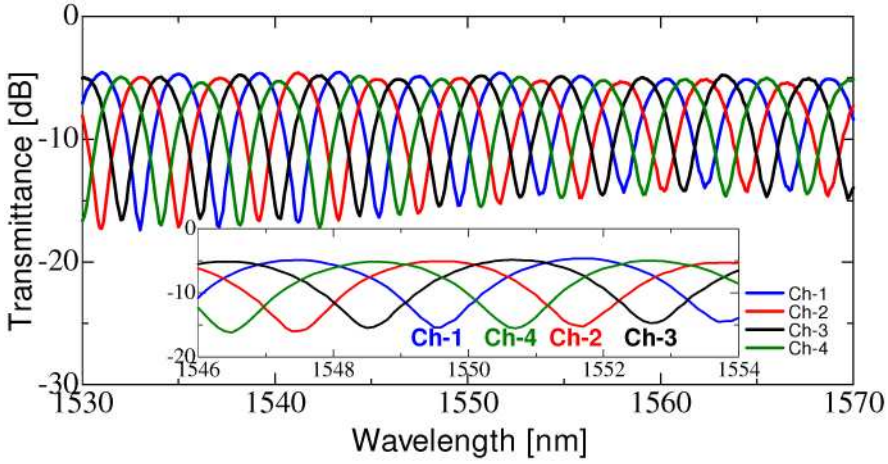

Fig. 14. Measured transmission spectra of the delayed interferometer integrated Type-II scheme. Inset shows the magnified views at around λ=1.55 μm.

Figure 14 shows the measured transmission spectra when an optical signal is incident on the delayed interferometer integrated 90° hybrids (see Fig. 13) employing the Type-II scheme. We were able to observe successful quadrature phase behavior of the fabricated device within the C-band spectral range. Each output transmittance of the device sinusoidally varies in accordance with the phase differences at the delayed interferometers. As seen in the inset in Fig. 14, π-phase differences were clearly observed at the In-phase channels (Ch-1 and 2) and the Quadrature channels (Ch-3 and 4) for the Type-II scheme, which means that the optical demodulation by coupling to balanced PDs is never accompanied by any waveguide intersections.

#121211 - $15.00 USD Received 9 Dec 2009; revised 24 Dec 2009; accepted 30 Dec 2009; published 17 Feb 2010

Then, we characterized a common-mode rejection ratio (CMRR), which is a measure of the electrical power balance to each output channels of the 90° hybrid. In this work, for convenience, we characterized the CMRR by measuring the optical power balance to each output channel of the 90-deg hybrids. Figure 15 shows the CMRRs for the In-phase and the Quadrature channels of the fabricated Type-II scheme. Both for the In-phase and the Quadrature channels, the CMRR of >20 dB was measured over the C-band spectral range, which satisfies the typical system requirement [9].

Figure 16 shows the experimentally estimated relative phase deviation ($\Delta\phi$) of the Type-II scheme. As seen in Fig. 16, $\Delta\phi$ was measured to be less than ±5° for each output channel which quantitatively agrees well with the calculation result shown in Fig. 9(b).

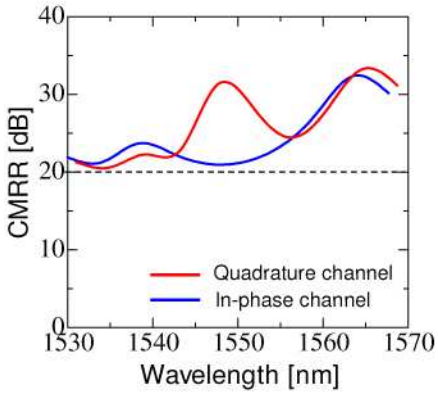

Fig. 15. Experimentally characterized CMRRs for the In-phase channels and the Quadrature channels of the Type-II scheme

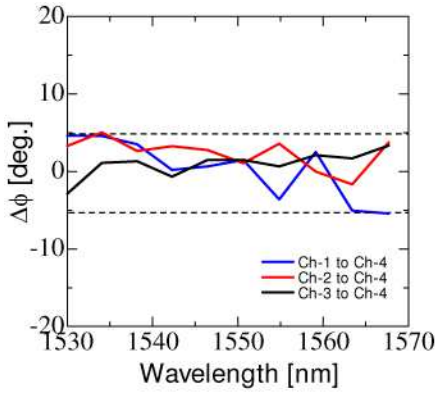

Fig. 16. Experimentally estimated relative phase deviation ($\Delta\phi$) for the Type-II scheme

Figure 17 shows the constellation diagrams for the Type-II scheme within the C-band spectral range. In this case, the constellation diagram corresponds to the distributions of complex amplitudes in the complex plane. In other words, the vertical amplitudes of the depicted constellation diagram for each axis correspond to the wavelength sensitivity of transmittances for each output channel in the Type-II scheme. The horizontal amplitudes of the depicted constellation diagram for each axis correspond to $\Delta\phi$ for each output channel in the Type-II scheme. Also, the degree of circularity of the depicted constellation diagram indicates the interchannel imbalance for each output channel in the Type-II scheme. In Fig. 17, we were able to estimate the wavelength sensitive loss of <0.9dB, $\Delta\phi$ of <5°, and the interchannel imbalance of <0.7dB over the C-band spectral range.

#121211 - $15.00 USD Received 9 Dec 2009; revised 24 Dec 2009; accepted 30 Dec 2009; published 17 Feb 2010

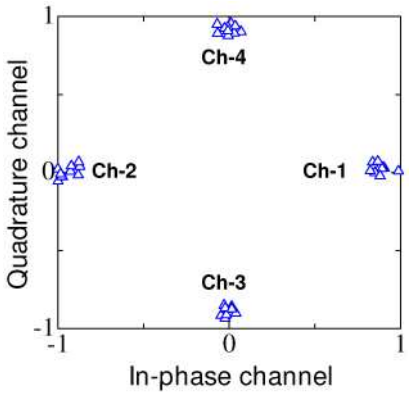

Fig. 17. Constellation diagrams for the Type-II scheme within the C-band spectral range. In this case, complex amplitudes were obtained from the experimental data shown in Fig. 14.

5. Discussion on taper shape

In this work, we used the linear-tapered 2 × 4 MMI coupler for the phase control at the output channels and the reduction of the MMI length. The aforementioned two contributions are not restricted to the linear-tapered MMI structure. In other words, if we adjust the MMI taper parameters of the tapered 2×4 MMI coupler to satisfy the phase matching condition, we can achieve similar results shown in Figs. 14 ~ 17. As a matter of course, the optimized MMI taper parameters become different depending on the modulation function of the tapered 2×4 MMI coupler.

Table 1 shows $W_M(z)$, $\langle\beta_0-\beta_v\rangle$, proportional constant χ^{SQ}, the optimized χ^{SQ} for satisfying the phase matching condition for the Type-II scheme employing a parabolic-tapered 2 × 4 MMI coupler. Similarly, Table 2 shows the same parameters shown in Table 1 for the Type-II scheme employing an exponential-tapered 2×4 MMI coupler.

Table 1. Calculated $W_M(z)$, $\langle\beta_0-\beta_v\rangle$, proportional constant χ^{SQ}, the optimized χ^{SQ} for satisfying the phase matching condition for the Type-II scheme employing a parabolic-tapered 2×4 MMI coupler

	Parabolic-tapered 2×4 MMI coupler
$W_M(z)$	$W_M(z) = W_{MS} + (W_{MF} - W_{MS}) \cdot \left(\frac{z}{L_{S24}}\right)^2$
$\langle\beta_0-\beta_v\rangle$	$\langle \beta_0 - \beta_v \rangle = \frac{\nu(\nu+2)\pi\lambda}{4 \cdot N_{eq} \cdot W_{MF}^2} \chi^{SQ}$
Proportional constant (χ^{SQ})	$\chi^{SQ} = \frac{W_{MF}}{2}\left(\frac{1}{W_{MS}} + \frac{W_{MF} \tanh^{-1}\left[\sqrt{\frac{-W_{MF}+W_{MS}}{W_{MS}}}\right]}{W_{MS}\sqrt{W_{MS}}\sqrt{-W_{MF}+W_{MS}}}\right)$
Optimized χ^{SQ} for the phase matching	$\chi^{SQ} = 1.74$

#121211 - $15.00 USD Received 9 Dec 2009; revised 24 Dec 2009; accepted 30 Dec 2009; published 17 Feb 2010

Table 2. Calculated $W_M(z)$, $<\beta_0-\beta_v>$, proportional constant χ^{EXP}, the optimized χ^{EXP} for satisfying the phase matching condition for the Type-II scheme employing an exponential-tapered 2×4 MMI coupler

	Exponential-tapered 2×4 MMI coupler
$W_M(z)$	$W_M(z) = W_{MS} + (W_{MF} - W_{MS}) \cdot \left(\frac{Exp(z / L_{S24}) - 1}{e - 1} \right)$
$<\beta_0-\beta_v>$	$\langle \beta_0 - \beta_v \rangle = \frac{\nu(\nu+2)\pi\lambda}{4 \cdot N_{eq} \cdot W_{MF}^2} \chi^{EXP}$
Proportional constant (χ^{EXP})	$\chi^{EXP} = \frac{(e-1)W_{MF}\left(W_{MF}^2 - 2W_{MS}W_{MF} + e \cdot W_{MS}^2 - (e-1)W_{MS}W_{MF}\log(W_{MF}/W_{MS})\right)}{W_{MS}(W_{MF} - e \cdot W_{MS})^2}$
Optimized χ^{EXP} for the phase matching	$\chi^{EXP} = 1.79$

As can be seen in Tables 1 and 2, each taper shape ($W_M(z)$) and proportional constant (χ) are systematically determined by arbitrary W_{MS} and W_{MF}, thus enabling to determine the appropriate MMI length depending on the MMI taper shapes. In order to operate each device as the optical 90° hybrid without using the extra phase shifter, the parameters of W_{MS} and W_{MF} should be optimized for each χ to satisfy the phase matching relation shown in Tables 1 and 2.

6. Summary

We proposed, theoretically analyzed and experimentally demonstrated a novel 90° hybrid based on the PI-based tapered 2×4 MMI coupler serially connected by the 2×2 MMI coupler, and discussed its potential for use in a coherent receiver monolithically integrated with balanced photodiodes. Based on the theoretical considerations, the proposed 90° hybrid was fabricated and characterized. The proposed 90° hybrid was realized in the deep-ridge waveguide with a GaInAsP/InP material system. The device length of the proposed 90° hybrid was 227 μm. Unlike the case of the conventional 4×4 MMI coupler, the In-phase and the Quadrature phase responses were observed at each mutually adjacent output waveguide in the proposed device, which makes it possible to implement coherent detection without any waveguide intersections between the 90° hybrid and the balanced PDs. The fabricated proposed 90° hybrid exhibited a wavelength sensitive loss of <0.9dB, a CMRR of >20dB, and a relative phase deviation ($\Delta\phi$) of <±5° over the C-band spectral range.

#121211 - $15.00 USD Received 9 Dec 2009; revised 24 Dec 2009; accepted 30 Dec 2009; published 17 Feb 2010